HHS Public Access

Author manuscript

Chem Mater. Author manuscript; available in PMC 2021 April 14.

Published in final edited form as:

Chem Mater. 2019 January 8; 31(1): 251–259. doi:10.1021/acs.chemmater.8b04333.

Gadolinium Doping Enhances the Photoacoustic Signal of Synthetic Melanin Nanoparticles: A Dual Modality Contrast Agent for Stem Cell Imaging

Jeanne E. Lemaster[†,◆], **Zhao Wang**[‡,⊥,◆], **Ali Hariri**[†], **Fang Chen**[†,§], **Ziying Hu**[‡,⊥], **Yuran Huang**[‡,⊥], **Christopher V. Barback**[‖], **Richard Cochran**[‡,○], **Nathan C. Gianneschi**[‡,⊥,#,▽], **Jesse V. Jokerst**[*,†,§,‖]

[†]Department of NanoEngineering, University of California San Diego, 9500 Gilman Drive, La Jolla, California 92093, United States

[‡]Department of Chemistry and Biochemistry, University of California San Diego, 9500 Gilman Drive, La Jolla, California 92093, United States

[§]Materials Science and Engineering Program, University of California San Diego, 9500 Gilman Drive, La Jolla, California 92093, United States

[‖]Department of Radiology, University of California San Diego, 9500 Gilman Drive, La Jolla, California 92093, United States

[⊥]Department of Chemistry, Northwestern University, 2145 Sheridan Road, Evanston, Illinois 60208, United States

[#] Department of Materials Science & Engineering, Northwestern University, 2145 Sheridan Road, Evanston, Illinois 60208, United States

[▽]Department of Biomedical Engineering, Northwestern University, 2145 Sheridan Road, Evanston, Illinois 60208, United States

Abstract

In this paper, we show that gadolinium-loaded synthetic melanin nanoparticles (Gd(III)-SMNPs) exhibit up to a 40-fold enhanced photoacoustic signal intensity relative to synthetic melanin alone and higher than other metal-chelated SMNPs. This property makes these materials useful as dual labeling agents because Gd(III)-SMNPs also behave as magnetic resonance imaging (MRI)

[*]**Corresponding Author** jjokerst@ucsd.edu.

[○]Present Address

Currently affiliated with Thermo Fisher Scientific, Analytical Instrumentation Group (R.C.).

◆J.E.L. and Z.W. contributed equally to this work.

Author Contributions

The manuscript was written through contributions of all authors. All authors have given approval to the final version of the manuscript.

Supporting Information

The Supporting Information is available free of charge on the ACS Publications website at DOI: 10.1021/acs.chemmater.8b04333.

TEM images, DLS data, absorbance of Gd(III) solution, PA intensity of other lanthanide-doped SMNPs, PA stability data, MRI data, subcutaneous PA injection data, toxicity assays, additional STEM and optical microscopy images, and additional TEM of SMNP internalization by hMSCs (PDF)

Intensity increase upon addition of Gd(III) (AVI)

The authors declare no competing financial interest.

contrast agents. As a proof-of-concept, we used these nanoparticles to label human mesenchymal stem cells. Cellular uptake was confirmed with bright-field optical and transmission electron microscopy. The Gd(III)-SMNP-labeled stem cells continued to express the stem cell surface markers CD73, CD90, and CD105 and proliferate. The labeled stem cells were subsequently injected intramyocardially in mice, and the tissue was observed by photoacoustic and MR imaging. We found that the photoacoustic signal increased as the cell number increased (R^2 = 0.96), indicating that such an approach could be employed to discriminate between stem cell populations with a limit of detection of 2.3×10^4 cells in in vitro tests. This multimodal photoacoustic/MRI approach combines the excellent temporal resolution of photoacoustics with the anatomic resolution of MRI.

Graphical Abstract

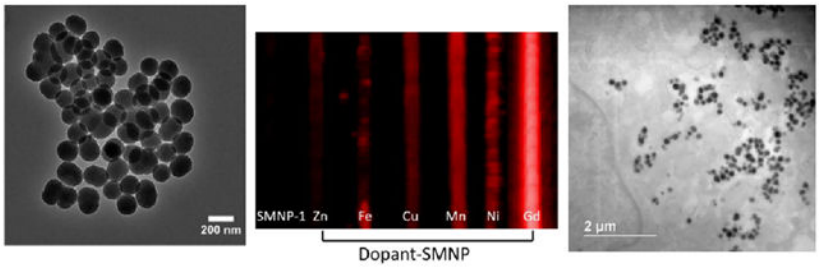

1. INTRODUCTION

Melanin is a natural pigment with myriad functions arising from its chemical structure including metal ion chelation, photoprotection, free radical quenching, and coloration.[1-5] In humans, melanins can serve as a biomarker for melanoma[6,7] and Parkinson's disease.[8] To exploit these properties, several groups have reported synthetic melanin nanoparticles (SMNPs) synthesized by auto-oxidation of dopamine or *L*-3,4-dihydroxyphenylalanine.[4,9] These materials have also been employed as contrast agents.[10-12] For example, SMNPs loaded with paramagnetic iron can act as efficient contrast agents for T_1-weighted magnetic resonance imaging (MRI).[13,14] SMNPs also have a strong optical absorption in the near-infrared region,[12] and previous research has shown that melanins prepared from dopamine monomers provide photoacoustic (PA) signal.[15] Pristine and metal-doped polydopamine nanoparticles have shown excellent biocompatibility and biodegradeability and can be used for combined therapy such as phototherapy, drug delivery, and imaging[16-20]—including stem cell imaging.

Indeed, stem cell imaging is an important tool for monitoring cell-based therapies.[21,22] MRI is one of the most common modalities for imaging cells and typically utilizes ferromagnetic inorganic nanoparticles,[23-30] stable paramagnetic complexes,[31] or gadolinium (Gd)-based chelates.[32-34] However, MRI is limited by long temporal resolution; acoustic and photoacoustic imaging can overcome this limitation with video frame rates[35,36] Recently, we and others have reported photoacoustic cell imaging via Prussian blue-poly (1-lysine),[35] iron-oxide based nanobubbles with 1,1′-dioctadecyl-3,3,3′,3′-tetramethylindotricarbocyanine iodide,[37] exosome-like silica nanoparticles,[38] biodegradable

P_2O_5–CaO–Na_2O phosphate-based glass nanospheres,[39] and phosphorylcholine-coated semiconducting polymers.[40] However, a multimodal probe with both MRI and photoacoustic imaging would have significant utility. Real-time photoacoustic imaging would provide a means for monitoring delivery, and deep tissue MRI would be used in tandem to provide longer-term follow-up of stem cell location and quantities, superimposed with anatomical information.

Thus, we prepared SMNPs via polymerization of dopamine in the presence of Mn(III) using a recently developed metal-templated loading approach.[14] The data showed that using postmodification to chelate the Gd to the synthetic melanin particle surface led to a very low Gd-loading percentage; thus, we used the Mn displacement method for the synthesis of Gd-SMNPs to yield high and tunable Gd loadings.[14] We then displaced the Mn from SMNPs with gadolinium to yield a dual, MRI/photoacoustic contrast agent due to the lower binding affinity of Mn.[14,41] Surprisingly, the gadolinium-loaded particles exhibited dramatically enhanced photoacoustic contrast over metal-free SMNPs. We then prepared various metal-loaded SMNPs and investigated them for similar enhancements in photoacoustic contrast. We found that the photoacoustic signal of the SMNPs increases with incorporation of different metal ions with Gd(III), showing the highest signal intensities among SMNPs doped with Ni(II), Zn(II), Cu(II), Mn(III), or Fe(III). This discovery of enhanced photoacoustic signals due to gadolinium integration into the nanoparticles sets the stage for other multimodal imaging efforts.

2. METHODS

2.1. Reagents.

The following materials were acquired and used as received: dopamine hydrochloride (Sigma-Aldrich), potassium permanganate (Thermo Fisher), hydrochloride (Sigma-Aldrich), ethanol (Sigma-Aldrich), ammonia (Sigma-Aldrich), nitric acid (Sigma-Aldrich), Tris base (Sigma-Aldrich), phosphate-buffered saline (PBS; Thermo Fisher), matrigel (Corning), ultraPure agarose (Thermo Fisher), and dimethyl sulfoxide (DMSO, Sigma-Aldrich).

2.2. Instrumentation.

The size of the SMNPs was measured by dynamic light scattering (DLS) (Zetasizer-90, Malvern Instruments). Transmission electron microscopy (TEM) used a FEI Sphera microscope operating at 200 kV. Micrographs were recorded on a 2 K X2 KGatan CCD camera. Photoacoustic imaging was performed with a Vevo 2100 instrument (Visualsonics) with a 21 MHz-centered transducer as described previously.[42] This system utilizes a flashlamp pumped Q-switched Nd:YAG laser with an optical parameteric oscillator and a second harmonic generator with wavelengths of 680–970 nm with a 1 nm step size and a pulse of 4–6 ns. The peak energy is 45 ± 5 mJ at 20 Hz at the source, the field-of-view (FOV) is 14–23 mm, and the acquisition rate is 5 frames/s. The specimens were aligned at a depth of approximately 1 cm from the transducer. The laser was optimized prior to use with a built-in energy power software and meter. We used 100% laser energy with 10–20 dB gain and 21 MHz frequency. Photoacoustic spectra were collected from 680 to 970 nm, and three-dimensional scans were performed. The distance between the imaging transducer and

phantom was maintained constant in each of the scans. We collected eight fields-of-view for each specimen. Absorbance measurements used a Shimadzu UV-3600 spectrophotometer. The metal concentration for the initial doped SMNP synthesis was quantified by inductively coupled plasma-optical emission spectrometry (ICP-OES) using a PerkinElmer Optima 3000DV spectrometer. The metal concentration for MRI and Gd(III) retention was quantified by inductively coupled plasma-mass spectrometry (ICP-MS) using an Agilent 4500 series ICP-MS (Agilent Technology, Inc.).

2.3. SMNP Syntheses.

SMNPs were prepared from dopamine according to a previously published method.[43] In a typical reaction, 50 mL of deionized water and 20 mL of ethanol were fully mixed with 1.2 mL of ammonia (28–30%) under constant stirring at room temperature for 1 h. Then, 5 mL of dopamine hydrochloride aqueous solution (4 mg/mL) was quickly injected into this solution. The SMNPs were centrifuged and washed with deionized water three times to yield the final sample.

Metal-doped SMNPs were prepared according to published procedures.[13,14] Briefly, dopamine hydrochloride and metal salts were fully dissolved in 100 mL of deionized water under stirring at room temperature for 1 h. Subsequently, 50 mL of Tris aqueous (25 mM) solution was quickly injected into the solution. After another 1.5 h, the doped nanoparticles were centrifuged and washed three times with deionized water[13] at neutral pH. Gd(III)-doped SMNPs were prepared by employing an additional step using Mn(III)-doped SMNPs: [13] 60 mg of $GdCl_3$ was added to 10 mL of Mn(III)-doped SMNPs (2 mg/mL in solution) and stirred at room temperature overnight, separated by centrifugation, and washed three times with deionized water. To calculate the metal loading in the final product, an aliquot of each sample was added to a concentrated HNO_3 solution for overnight digestion. The solution was then diluted to 10 mL (1% HNO_3) and analyzed by inductively coupled plasma-optical emission spectroscopy (ICP-OES). The solution for MRI was digested in aqua regia for 1 h, diluted to 10 mL (2% HNO_3), and analyzed by inductively coupled plasma-mass spectroscopy (ICP-MS).

2.4. Cell Culture.

Poietic human mesenchymal stem cells (hMSCs; Lonza, PT-2501) were grown in supplemented media (Lonza, PT-3001) and seeded in a T75 flask at a concentration of 5000 cells/cm^2. These cells were labeled with nanoparticles and incubated under standard conditions. The hMSCs were washed three times with PBS to remove free nanoparticles and detached using TrypLE Express (Life Technologies). Cell viability was determined using 3-(4,5-dimethylthiazol-2-yl)-2,5-diphenyltetrazolium bromide for the MTT assay (Biotium). Then, 10 μL of MTT solution was added to 100 μL of medium in each well, mixed briefly, and incubated at 37 °C for 4 h. Then, 200 μL of DMSO was added to each well and pipetted to dissolve the resulting formazan salt. Absorbance was measured to 570 nm. The MTT assays were conducted by plating 8000 cells per well in replicate ($n = 8$) in a 96 well plate and treated at varying timepoints (0–24 h) at a constant concentration (0.42 mg/mL) as well as at varying concentrations (0–0.84 mg/mL) at a constant time (4 h) unless otherwise noted. The wells were analyzed in replicate ($n = 8$).

2.5. In Vitro Photoacoustic Imaging and MRI.

For photoacoustic imaging of hMSCs, cells were labeled with nanoparticles and mixed in a 1% agar solution. The gain was set to 10–20 dB and read at a wavelength of 720 nm. Eight fields of view were collected for each sample. To measure the relaxivity of the Gd-SMNPs, various concentrations of Gd-SMNPs from 0 to 0.46 mM were prepared in a 1% agar solution. For the 4.7 T MRI, we used a MRS 4000 system from MR Solutions with a variable strength electromagnet set to 4.7 T. After scouting, we acquired T1 spin echo multislice images with horizontal phase encoding directions, FOVs of 60 mm, an echo time of 11 ms, a repetition time of 720 ms, a flip angle of 90°, a 512 × 512 matrix, and autogain calibration. We acquired 12 slices with 1 mm thickness. The ϕ and θ angles were set to zero for coronal slices with no echo asymmetry. The T1 reciprocal was plotted as a function of concentration from 0.046 to 0.46 mM. For the 7 T MRI, we used a Bruker 7.0 T magnet with Avance II hardware. After scouting, we acquired T1 spin echo multislice images with horizontal phase encoding directions, FOVs of 6.91/3.12 cm, an echo time of 1/1, a repetition time of 750 ms, a flip angle of 90°, and a 256 × 116 matrix. We acquired 6 slices with 2 mm thickness. The T1 reciprocal was plotted as a function of concentration from 0.046 to 0.46 mM.

2.6. In Vivo Photoacoustic Imaging and MRI.

For imaging, 500 000 Gd(III)-SMNP-labeled hMSCs were injected in a 50% matrigel mixture in the left ventricle (LV) wall of nude mice. Control mice were injected with a PBS/matrigel solution only. Echocardiograms were performed in the long axis (lax) mode. MRI was performed before injection and 15 min after injection with labeled hMSCs.

2.7. Data Analysis.

ImageJ 1.48 v58 was used to quantitate the photoacoustic signal for the SMNPs via region of interest (ROI) analysis for the average integrated density in arbitrary units (bit depth) using the maximum intensity projection for 8-bit images.[44] The photoacoustic means and standard deviations were calculated from eight fields-of-view in each sample. The error bars represent the standard deviation of the measurements unless otherwise noted.

3. RESULTS AND DISCUSSION

3.1. Synthesis and Characterization.

Three types of SMNPs were used in these studies: (1) SMNPs prepared by polymerization of dopamine (SMNP);[43] (2) metal-doped SMNPs made by polymerization of dopamine in the presence of metal salts; and (3) Gd(III)-doped SMNPs made via a metal exchange method beginning with Mn(III)-doped SMNPs as a template (Figure 1).[13,14] The synthesis began with the polymerization of dopamine (Figure 1A,B) to form spherical particles. Previous research has shown that the higher metal binding capacities and faster binding rates of synthetic melanin nanoparticles than melanin polymers are due to the higher surface area to volume ratio.[9] The morphology of these nanoparticles was characterized by transmission electron microscopy (TEM) (Figure 1C,D, and Supporting Information Figure S1). All samples were spherical and monodisperse: Dynamic light scattering (DLS) (Figure 1, and

Supporting Information Figure S2) showed that the size of the SMNPs was 150 nm with a polydispersity index (PDI) of 0.11 ± 0.03 (Figure 1E). The size of the Gd(III)-doped SMNPs was 160 nm with a PDI of 0.18 ± 0.03 (Figure 1F).

The concentration of metals ranged from 5.9 to 8.3% by weight with respect to polydopamine as determined by ICP-OES (Table 1). Although the synthetic conditions were optimized for achieving uniform size and high loadings, there were slight variations in particle size and metal loading concentration. This is likely due to the changes in affinities and coordination geometries between dopamine and different metal ions that may significantly affect polymerization kinetics.[45] The ζ-potential of Mn-SMNPs was −10.7 mV, whereas the ζ-potential of the Gd(III)-doped SMNPs was −9.5 mV.

3.2. Photoacoustic and MRI Performance.

The photoacoustic spectra of SMNPs and metal-doped (Ni(II), Zn(II), Cu(II), Mn(III), Fe(III), and Gd(III)) SMNPs indicated a broad peak across all samples from 720 to 760 nm (Figure 2A) with Gd(III)-SMNPs showing the highest photoacoustic intensity amongst all samples from 680 to 850 nm. Photoacoustic imaging at 720 nm of SMNPs and metal-doped SMNPs (Figure 2B,C) showed that the gadolinium-based material exhibited the highest photoacoustic signal intensity at neutral pH (all samples were 0.58 mg/mL with respect to polydopamine). This effect correlates with absorbance spectroscopy, where Gd(III)-SMNPs exhibit the strongest absorbance from 700 to 900 nm (Figure 2D). Miao et al. also showed that metal-chelated polydopamine nanoparticles show higher absorbance than polydopamine nanoparticles between 700 and 900 nm.[46] Importantly, a solution of $GdCl_3$ alone (no nanoparticles) had no absorbance (Supporting Information Figure S3). Other lanthanides also produce a photoacoustic signal increase relative to metal-free SMNPs (Figure S4). The Ce-doped SMNPs had the highest photoacoustic signal of $6 \times 10^4 \pm 1 \times 10^3$ au, whereas Er-doped SMNPs had the lowest photoacoustic signal of $9 \times 10^4 \pm 8 \times 10^2$ au; however, Gd was used for further studies because Gd-based contrast agents also have high MRI signals.[32-34] Additionally, lanthanide-doped nanoparticles have been used in luminescence imaging due to long luminescence lifetimes, large ranges of upconversion luminescence wavelengths, and high signal-to-noise ratios.[47]

To further understand the activatable nature of this phenomenon, we monitored the photoacoustic signal in real time while adding Gd(III) to the manganese-loaded nanoparticles (Figure 2E). In aqueous solution, Gd(III) has low absorbance from 400 to 900 nm (Supporting Information Figure S3). We initially observed a 2-fold intensity increase upon addition of Gd(III) (Figure 2F); the signal increased 16-fold with further mixing (Figure 2G, and Supporting Information Video 1).

To evaluate stability, photoacoustic signal from SMNPs was studied under continuous laser irradiation (pulse duration of 5 ns; 0.167 s between pulses) and showed a constant signal over 15 min. The signal difference between the first 100 frames and the last 100 frames is 6.6%, indicating that the SMNPs are stable under photoacoustic irradiation (Supporting Information Figure S5A).

The photoacoustic signal intensity of Gd(III)-doped SMNPs is dependent on the concentration of both SMNPs and Gd(III). The Gd(III)-doped SMNPs were measured from 0.068 to 0.68 mg/mL of nanoparticles and exhibited a linear increase (R^2 = 0.96) with increasing SMNP concentration (Figure 3A). Methylene blue (MB, 0.4 mM) was a positive control,[48,49] and deionized water and Gd(III) solution (40 mg/mL) in water were negative controls. At higher concentrations of SMNPs, the photoacoustic intensity with respect to SMNPs continued to increase linearly from 0 to 3.5 mg/mL with R^2 = 0.98 (Supporting Information Figure S5B).

This photoacoustic signal enhancement is likely due to an improved absorption cross-section via melanin coordination of the metal ions via catechol groups—this leads to increased absorption.[50] Indeed, the absorption (Supporting Information Figure S5C) was higher for 5 and 10% Gd-SMNPs than Mn-SMNPs and 0.5–2% Gd-SMNPs. The photoacoustic signal (Figure 3B) also increased with Gd(III) loading when the SMNP concentration was held constant. Photoacoustic signal is proportional to concentration. Related work has shown the presence of vinylene bonds can increase the mass absorption coefficient and photothermal conversion efficacy in polymers.[51] Related work has increased the photoacoustic signal of nanoparticles via the addition of a silica coat to gold nanorods or semiconductor polymer nanoparticles. This is because the silica shell has a lower thermal conductivity and heat capacity than water. Thus the coated particles achieve a higher temperature than bare particles, leading to a higher thermal gradient and a higher photoacoustic signal.[52-54]

Gd(III)-SMNPs were also studied in terms of MRI parameters. The r_1 was 3.35 and 2.90 mM^{-1} s^{-1} for 4.7 and 7.0 T fields, respectively (Supporting Information Figure S6A-D). These values are similar to commercially available agents, Gd-DOTA and Gd-DTPA.[55,56] Additionally, Gd(III)-SMNP subcutaneous injections were performed in mice (Supporting Information Figure S6E,F), showing enhanced photoacoustic signal after injection with Gd(III)-SMNPs.

3.3. Cellular Imaging.

The hMSC uptake of Gd(III)-SMNPs was measured to determine the optimal concentration and time for cell labeling.[57,58] The photoacoustic intensity was quantified for 1.5×10^5 cells treated with 0–0.84 mg/mL of Gd(III)-SMNPs at 8 h of incubation time (Figure 4A). No further increase was seen after 0.42 mg/mL. We then studied the effect of time. The photoacoustic intensity of 1.5×10^5 cells treated with 0.42 mg/mL of Gd(III)-SMNPs at varying time periods (1–24 h) was quantified (Figure 4B). The hMSCs labeled with 0.42 mg/mL Gd-SMNPs had an 8-fold higher photoacoustic signal than hMSCs labeled with 0.1 mg/mL Gd-SMNPs. hMSCs labeled for 4 h with Gd-SMNPs showed a 3-fold higher photoacoustic intensity than cells treated for 1 h with Gd-SMNPs ($p < 0.05$). An MTT assay revealed no significant difference (p-value >0.05) in the cell viability of cells treated with up to 0.84 mg/mL of Gd(III)-SMNPs (Supporting Information Figure S7), suggesting good biocompatibility.[59] Therefore, 4 h of incubation with 0.42 mg/mL of Gd(III)-SMNPs was determined to be the optimal incubation time without adverse effects on cell viability. Our prior work showed that there was no significant release of the Gd(III) ion from the SMNP over 7 days after incubation with $CaCl_2$ and $ZnCl_2$ solutions for 7 days as measured by ICP.

[14] We repeated this experiment and found that 97.9% of Gd(III) was retained in the particle after 7 days of incubation in water at room temperature as measured by ICP.

Dark-field scanning transmission electron microscopy (STEM), transmission electron microscopy (TEM), and bright-field microscopy were used to confirm the uptake of Gd(III)-SMNPs in hMSCs (Figure 4C,D and Supporting Information Figures S8 and S9). Previous studies have shown mesoporous silica uptake in hMSCs from 1 to 4 h,[60] similar to our observed uptake of Gd(III)-SMNPs in hMSCs. Parameters such as charge, composition, surface reactivity, and surface adsorption have been implicated in affecting the time of nanoparticle uptake in cells.[61] Polydopamine-containing nanoparticles have shown good biocompatibility and are cleared from the body via the reticuloendothelial system.[16] PEGylation was not necessary because intravenous injection was not performed; the cells were labeled with the nanoparticles ex vivo, and the cells were then implanted into the myocardium. Photoacoustic images and imaging intensity of 0–200 K cells indicated a linear relationship ($R^2 = 0.96$) between cell number and photoacoustic intensity (Figure 4E,F). The lowest number of cells we measured was 5.0×10^4, and we calculated the lowest detectable number of cells to be 2.3×10^4 based on three standard deviations above the background mean. Previous research reported cell detection limits varying from single cells—10×10^4 cells in MRI and photoacoustic imaging.[42,62,63] However, achieving ultralow detection limits is rarely clinically useful because human trials routinely use 10^6–10^8 cells.[64-66]

We next conducted additional studies to understand what effects labeling has on the cells' biology. CD73, CD90, and CD105 were used as hMSC marker proteins for flow cytometry analysis. Analysis showed that the labeled hMSCs still express these three stem cell surface markers (Supporting Information Figure S10A-C). However, the expression of CD90 in the labeled cells was 16% less than the expression of CD73 in the control cells, suggesting that the SMNP labeling may be affecting the expression of CD73. The proliferation of unlabeled and labeled hMSCs was also measured over time. hMSCs were labeled by incubation with Gd(III)-SMNPs for 4 h. Cells continued to proliferate for 3 weeks after labeling with the nanoparticles (Supporting Information Figure S8E). Although labeled cells proliferated approximately 26% slower than the unlabeled hMSCs, both the labeled and unlabeled hMSCs doubled in approximately 3 days (Supporting Information Figure S11). Although chelation increases the biocompatibility of Gd-based agents,[67] it is possible that free Gd is present, as cells internalize the particles, which may act for slow proliferation and affect the expression of marker proteins.[59]

Finally, in vivo experiments using 500 000 cells labeled with Gd(III)-SMNPs were performed in mice (Figure 5). Bone marrow mononuclear cells have been found to promote heart function and neovascularisation after myocardial infarction via intramyocardial injection delivery.[68] Echocardiograms pre- and immediately post-injection are also shown in Figure 5 and indicate that the photoacoustic signal increased 64-fold +11.3. Transverse MRI images pre- and post-injection show that the MRI signal increased 2.0-fold ±0.17 versus baseline (Figure 5C,D).

4. CONCLUSIONS

This study details a synthetic melanin-based contrast agent for photoacoustic imaging and MRI. The most important finding is that the photoacoustic intensity increased dramatically upon incorporation of metal ions into polydopamine-based nanoparticles. Chelation is known to increase the biocompatibility of Gd-based contrast agents[67] that are clinically used in MRI.[69,70] We used the Gd(III)-enhanced photoacoustic signal to image stem cells, in vivo coupling this modality with MRI. The labeled stem cells still expressed stem cell surface markers and continued to proliferate.

Supplementary Material

Refer to Web version on PubMed Central for supplementary material.

Acknowledgments

Funding

J.E.L. acknowledges funding from the National Institutes of Health (NIH) Institutional National Research Service Award T32 CA153915, Cancer Researchers in Nanotechnology. J.V.J. acknowledges funding from the NIH (Grants R00 HL117048 and DP2 HL137187) and infrastructure from Grant S10 OD021821. This work was performed, in part, at the San Diego Nanotechnology Infrastructure of UCSD, a member of the National Nanotechnology Coordinated Infrastructure, which is supported by the National Science Foundation (Grant ECCS-1542148). This work made use of the EPIC facility of Northwestern University's NUANCE Center, which has received support from the Soft and Hybrid Nanotechnology Experimental (SHyNE) Resource (NSF ECCS-1542205); the MRSEC program (NSF DMR-1121262) at the Materials Research Center; the International Institute for Nanotechnology (IIN); the Keck Foundation; and the State of Illinois, through the IINNotes.

ABBREVIATIONS

DMSO	dimethyl sulfoxide
hMSCs	human mesenchymal stem cells
ICP-OES	inductively coupled plasma-optical emission spectrometry
ICP-MS	inductively coupled plasma-mass spectrometry
PBS	phosphate-buffered saline
Lu	lung
LV	left ventricle
SMNPs	synthetic melanin nanoparticles
STEM	scanning transmission electron microscopy
TEM	transmission electron microscopy

REFERENCES

(1). Simon JD; Peles DN The Red and the Black. Acc. Chem. Res 2010, 43, 1452–1460. [PubMed: 20734991]

(2). Meredith P; Sarna T The Physical and Chemical Properties of Eumelanin. Pigm. Cell Res 2006, 19, 572–594.

(3). Simon JD Spectroscopic and Dynamic Studies of the Epidermal Chromophores Trans-Urocanic Acid and Eumelanin. Acc. Chem. Res 2000, 33, 307–313. [PubMed: 10813875]

(4). Xiao M; Li Y; Zhao J; Wang Z; Gao M; Gianneschi NC; Dhinojwala A; Shawkey MD Stimuli-Responsive Structurally Colored Films from Bioinspired Synthetic Melanin Nanoparticles. Chem. Mater 2016, 28, 5516–5521.

(5). Xiao M; Li Y; Allen MC; Deheyn DD; Yue X; Zhao J; Gianneschi NC; Shawkey MD; Dhinojwala A Bio-Inspired Structural Colors Produced Via Self-Assembly of Synthetic Melanin Nanoparticles. ACS Nano 2015, 9, 5454–5460. [PubMed: 25938924]

(6). Zhang R; Fan Q; Yang M; Cheng K; Lu X; Zhang L; Huang W; Cheng Z Engineering Melanin Nanoparticles as an Efficient Drug–Delivery System for Imaging-Guided Chemotherapy. Adv. Mater 2015, 27, 5063–5069. [PubMed: 26222210]

(7). Horikoshi T; Ito S; Wakamatsu K; Onodera H; Eguchi H Evaluation of Melanin-Related Metabolites as Markers of Melanoma Progression. Cancer 1994, 73, 629–636. [PubMed: 8299084]

(8). Schwarz ST; Rittman T; Gontu V; Morgan PS; Bajaj N; Auer DP T1-Weighted Mri Shows Stage-Dependent Substantia Nigra Signal Loss in Parkinson's Disease. Mov. Disord 2011, 26, 1633–1638. [PubMed: 21491489]

(9). Kim DJ; Ju K-Y; Lee J-K The Synthetic Melanin Nanoparticles Having an Excellent Binding Capacity of Heavy Metal Ions. Bull. Korean Chem. Soc 2012, 33, 3788–3792.

(10). Ju K-Y; Lee JW; Im GH; Lee S; Pyo J; Park SB; Lee JH; Lee J-K Bio-Inspired, Melanin-Like Nanoparticles as a Highly Efficient Contrast Agent for T1-Weighted Magnetic Resonance Imaging. Biomacromolecules 2013, 14, 3491–3497. [PubMed: 23987128]

(11). Liu Y; Ai K; Liu J; Deng M; He Y; Lu L Dopamine-Melanin Colloidal Nanospheres: An Efficient near-Infrared Photothermal Therapeutic Agent for in Vivo Cancer Therapy. Adv. Mater 2013, 25, 1353–1359. [PubMed: 23280690]

(12). Li Y; Jiang C; Zhang D; Wang Y; Ren X; Ai K; Chen X; Lu L Targeted Polydopamine Nanoparticles Enable Photoacoustic Imaging Guided Chemo-Photothermal Synergistic Therapy of Tumor. Acta Biomater. 2017, 47, 124–134. [PubMed: 27721008]

(13). Li Y; Xie Y; Wang Z; Zang N; Carniato F; Huang Y; Andolina CM; Parent LR; Ditri TB; Walter ED; et al. Structure and Function of Iron-Loaded Synthetic Melanin. ACS Nano 2016, 10, 10186–10194. [PubMed: 27802021]

(14). Wang Z; Carniato F; Xie Y; Huang Y; Li Y; He S; Zang N; Rinehart JD; Botta M; Gianneschi NC High Relaxivity Gadolinium-Polydopamine Nanoparticles. Small 2017, 13, No. 1701830.

(15). Repenko T; Fokong S; De Laporte L; Go D; Kiessling F; Lammers T; Kuehne AJ Water-Soluble Dopamine-Based Polymers for Photoacoustic Imaging. Chem. Commun 2015, 51, 6084–6087.

(16). Liu X; Cao J; Li H; Li J; Jin Q; Ren K; Ji J Mussel-Inspired Polydopamine: A Biocompatible and Ultrastable Coating for Nanoparticles in Vivo. ACS Nano 2013, 7, 9384–9395. [PubMed: 24010584]

(17). Zhong X; Yang K; Dong Z; Yi X; Wang Y; Ge C; Zhao Y; Liu Z Polydopamine as a Biocompatible Multifunctional Nanocarrier for Combined Radioisotope Therapy and Chemotherapy of Cancer. Adv. Funct. Mater 2015, 25, 7327–7336.

(18). Lin L-S; Cong Z-X; Cao J-B; Ke K-M; Peng Q-L; Gao J; Yang H-H; Liu G; Chen X Multifunctional Fe3o4@ Polydopamine Core–Shell Nanocomposites for Intracellular Mrna Detection and Imaging-Guided Photothermal Therapy. ACS Nano 2014, 8, 3876–3883. [PubMed: 24654734]

(19). Liopo A; Su R; Oraevsky AA Melanin Nanoparticles as a Novel Contrast Agent for Optoacoustic Tomography. Photoacoustics 2015, 3, 35–43. [PubMed: 25893172]

(20). Yan J; Ji Y; Zhang P; Lu X; Fan Q; Pan D; Yang R; Xu Y; Wang L; Zhang L Melanin Nanoparticles as an Endogenous Agent for Efficient Iron Overload Therapy. J. Mater. Chem. B 2016, 4, 7233–7240. [PubMed: 32263725]

(21). Kircher MF; Gambhir SS; Grimm J Noninvasive Cell-Tracking Methods. Nat. Rev. Clin. Oncol 2011, 8, 677–688. [PubMed: 21946842]

(22). Wang J; Jokerst JV Stem Cell Imaging: Tools to Improve Cell Delivery and Viability. Stem Cells Int. 2016, 2016, No. 9240652. [PubMed: 26880997]

(23). Na HB; Song IC; Hyeon T Inorganic Nanoparticles for Mri Contrast Agents. Adv. Mater 2009, 21, 2133–2148.

(24). Laurent S; Forge D; Port M; Roch A; Robic C; Vander Elst L; Muller RN Magnetic Iron Oxide Nanoparticles: Synthesis, Stabilization, Vectorization, Physicochemical Characterizations and Biological Applications. Chem. Rev 2008, 108, 2064–2110. [PubMed: 18543879]

(25). Kraitchman DL; Heldman AW; Atalar E; Amado LC; Martin BJ; Pittenger MF; Hare JM; Bulte JW In Vivo Magnetic Resonance Imaging of Mesenchymal Stem Cells in Myocardial Infarction. Circulation 2003, 107, 2290–2293. [PubMed: 12732608]

(26). Li K; Ding D; Huo D; Pu KY; Thao NNP; Hu Y; Li Z; Liu B Conjugated Polymer Based Nanoparticles as Dual-Modal Probes for Targeted in Vivo Fluorescence and Magnetic Resonance Imaging. Adv. Funct. Mater 2012, 22, 3107–3115.

(27). Daldrup-Link HE; Rudelius M; Oostendorp RA; Settles M; Piontek G; Metz S; Rosenbrock H; Keller U; Heinzmann U; Rummeny EJ; et al. Targeting of Hematopoietic Progenitor Cells with Mr Contrast Agents. Radiology 2003, 228, 760–767. [PubMed: 12881578]

(28). Bulte JW; Douglas T; Witwer B; Zhang S-C; Strable E; Lewis BK; Zywicke H; Miller B; van Gelderen P; Moskowitz BM; et al. Magnetodendrimers Allow Endosomal Magnetic Labeling and in Vivo Tracking of Stem Cells. Nat. Biotechnol 2001, 19, 1141–1147. [PubMed: 11731783]

(29). Huang Y; Wei T; Yu J; Hou Y; Cai K; Liang X-J Multifunctional Metal Rattle-Type Nanocarriers for Mri-Guided Photothermal Cancer Therapy. Mol. Pharmaceutics 2014, 11, 3386–3394.

(30). Huang J; Bu L; Xie J; Chen K; Cheng Z; Li X; Chen X Effects of Nanoparticle Size on Cellular Uptake and Liver Mri with Polyvinylpyrrolidone-Coated Iron Oxide Nanoparticles. ACS Nano 2010, 4, 7151–7160. [PubMed: 21043459]

(31). Lauffer RB Paramagnetic Metal Complexes as Water Proton Relaxation Agents for Nmr Imaging: Theory and Design. Chem. Rev 1987, 87, 901–927.

(32). Caravan P; Ellison JJ; McMurry TJ; Lauffer RB Gadolinium(Iii) Chelates as Mri Contrast Agents: Structure, Dynamics, and Applications. Chem. Rev 1999, 99, 2293–2352. [PubMed: 11749483]

(33). Caravan P Strategies for Increasing the Sensitivity of Gadolinium Based Mri Contrast Agents. Chem. Soc. Rev 2006, 35, 512–523. [PubMed: 16729145]

(34). Aime S; Botta M; Terreno E Gd(Iii)-Based Contrast Agents for Mri. Adv. Inorg. Chem 2005, 57, 173–237.

(35). Kim T; Lemaster JE; Chen F; Li J; Jokerst JV Photoacoustic Imaging of Human Mesenchymal Stem Cells Labeled with Prussian Blue–Poly (L-Lysine) Nanocomplexes. ACS Nano 2017, 11, 9022–9032. [PubMed: 28759195]

(36). Weber J; Beard PC; Bohndiek SE Contrast Agents for Molecular Photoacoustic Imaging. Nat. Methods 2016, 13, 639–650. [PubMed: 27467727]

(37). Lemaster JE; Chen F; Kim T; Hariri A; Jokerst JV Development of a Trimodal Contrast Agent for Acoustic and Magnetic Particle Imaging of Stem Cells. ACS Appl. Nano Mater 2018, 1, 1321–1331.

(38). Chen F; Ma M; Wang J; Wang F; Chern S-X; Zhao ER; Jhunjhunwala A; Darmadi S; Chen H; Jokerst JV Exosome-Like Silica Nanoparticles: A Novel Ultrasound Contrast Agent for Stem Cell Imaging. Nanoscale 2017, 9, 402–411. [PubMed: 27924340]

(39). Foroutan F; Jokerst JV; Gambhir SS; Vermesh O; Kim H-W; Knowles JC Sol–Gel Synthesis and Electrospraying of Biodegradable (P2o5) 55–(Cao) 30–(Na2o) 15 Glass Nanospheres as a Transient Contrast Agent for Ultrasound Stem Cell Imaging. ACS Nano 2015, 9, 1868–1877. [PubMed: 25625373]

(40). Pu K; Shuhendler AJ; Valta MP; Cui L; Saar M; Peehl DM; Rao J Phosphorylcholine-Coated Semiconducting Polymer Nanoparticles as Rapid and Efficient Labeling Agents for in Vivo Cell Tracking. Adv. Healthcare Mater 2014, 3, 1292–1298.

(41). Larsson B; Tjälve H Studies on the Melanin-Affinity of Metal Ions. Acta Physiol. Scand 1978, 104, 479–484. [PubMed: 726939]

(42). Jokerst JV; Thangaraj M; Kempen PJ; Sinclair R; Gambhir SS Photoacoustic Imaging of Mesenchymal Stem Cells in Living Mice Via Silica-Coated Gold Nanorods. ACS Nano 2012, 6, 5920–5930. [PubMed: 22681633]

(43). Xiao M; Hu Z; Wang Z; Li Y; Tormo AD; Le Thomas N; Wang B; Gianneschi NC; Shawkey MD; Dhinojwala A Bioinspired Bright Noniridescent Photonic Melanin Supraballs. Sci. Adv 2017, 3, No. e1701151. [PubMed: 28929137]

(44). Abràmoff MD; Magalhães PJ; Ram SJ Image Processing with Imagej. Biophotonics Int. 2004, 11, 36–42.

(45). Wang Z; Xie Y; Li Y; Huang Y; Parent LR; Ditri T; Zang N; Rinehart JD; Gianneschi NC Tunable, Metal-Loaded Polydopamine Nanoparticles Analyzed by Magnetometry. Chem. Mater 2017, 29, 8195–8201.

(46). Miao Z-H; Wang H; Yang H; Li Z-L; Zhen L; Xu C-Y Intrinsically Mn2+-Chelated Polydopamine Nanoparticles for Simultaneous Magnetic Resonance Imaging and Photothermal Ablation of Cancer Cells. ACS Appl Mater. Interfaces 2015, 7, 16946–16952. [PubMed: 26196160]

(47). Lee SY; Lin M; Lee A; Park YI Lanthanide-Doped Nanoparticles for Diagnostic Sensing. Nanomaterials 2017, 7, 411.

(48). Kim C; Erpelding TN; Jankovic L; Pashley MD; Wang LV Deeply Penetrating in Vivo Photoacoustic Imaging Using a Clinical Ultrasound Array System. Biomed. Opt. Express 2010, 1, 278–284. [PubMed: 21258465]

(49). Song KH; Stein EW; Margenthaler JA; Wang LV Noninvasive Photoacoustic Identification of Sentinel Lymph Nodes Containing Methylene Blue in Vivo in a Rat Model. J. Biomed. Opt 2008, 13, No. 054033. [PubMed: 19021413]

(50). Ge R; Lin M; Li X; Liu S; Wang W; Li S; Zhang X; Liu Y; Liu L; Shi F; Sun H; Zhang H; Yang B Cu2+-Loaded Polydopamine Nanoparticles for Magnetic Resonance Imaging-Guided Ph- and near-Infrared-Light-Stimulated Thermochemotherapy. ACS Appl. Mater. Interfaces 2017, 9, 19706–19716. [PubMed: 28553876]

(51). Zhen X; Feng X; Xie C; Zheng Y; Pu K Surface Engineering of Semiconducting Polymer Nanoparticles for Amplified Photoacoustic Imaging. Biomaterials 2017, 127, 97–106. [PubMed: 28284105]

(52). Chen Y-S; Frey W; Kim S; Kruizinga P; Homan K; Emelianov S Silica-Coated Gold Nanorods as Photoacoustic Signal Nanoamplifiers. Nano Lett. 2011, 11, 348–354. [PubMed: 21244082]

(53). Repenko T; Rix A; Nedilko A; Rose J; Hermann A; Vinokur R; Moli S; Cao-Milàn R; Mayer M; von Plessen G; et al. Strong Photoacoustic Signal Enhancement by Coating Gold Nanoparticles with Melanin for Biomedical Imaging. Adv. Funct. Mater 2018, 28, No. 1705607.

(54). Lyu Y; Zeng J; Jiang Y; Zhen X; Wang T; Qiu S; Lou X; Gao M; Pu K Enhancing Both Biodegradability and Efficacy of Semiconducting Polymer Nanoparticles for Photoacoustic Imaging and Photothermal Therapy. ACS Nano 2018, 12, 1801–1810. [PubMed: 29385336]

(55). Sasaki M; Shibata E; Kanbara Y; Ehara S Enhancement Effects and Relaxivities of Gadolinium-Dtpa at 1.5 Versus 3 Tesla: A Phantom Study. Magn. Reson. Med. Sci 2005, 4, 145–149. [PubMed: 16462135]

(56). Tallury P; Santra S; Sharma P; De Castro M; Maria B; Bengtsson N; Biswas S; Saha AK; Walter GA; Scott EA Fluorescent and Paramagnetic Chitosan Nanoparticles That Exhibit High Magnetic Resonance Relaxivity: Synthesis, Characterization and in Vitro Studies. J. Biomed. Nanotechnol 2011, 7, 724–729. [PubMed: 22195491]

(57). Tseng C-L; Shih I-L; Stobinski L; Lin F-H Gadolinium Hexanedione Nanoparticles for Stem Cell Labeling and Tracking Via Magnetic Resonance Imaging. Biomaterials 2010, 31, 5427–5435. [PubMed: 20400176]

(58). Henning TD; Saborowski O; Golovko D; Boddington S; Bauer JS; Fu Y; Meier R; Pietsch H; Sennino B; McDonald DM Cell Labeling with the Positive Mr Contrast Agent Gadofluorine M. Eur. Radiol 2007, 17, 1226–1234. [PubMed: 17206428]

(59). Rogosnitzky M; Branch S Gadolinium-Based Contrast Agent Toxicity: A Review of Known and Proposed Mechanisms. BioMetals 2016, 29, 365–376. [PubMed: 27053146]

(60). Huang D-M; Hung Y; Ko B-S; Hsu S-C; Chen W-H; Chien C-L; Tsai C-P; Kuo C-T; Kang J-C; Yang C-S; et al. Highly Efficient Cellular Labeling of Mesoporous Nanoparticles in Human Mesenchymal Stem Cells: Implication for Stem Cell Tracking. FASEB J. 2005, 19, 2014–2016. [PubMed: 16230334]

(61). Zhao F; Zhao Y; Liu Y; Chang X; Chen C; Zhao Y Cellular Uptake, Intracellular Trafficking, and Cytotoxicity of Nanomaterials. Small 2011, 7, 1322–1337. [PubMed: 21520409]

(62). Stroh A; Faber C; Neuberger T; Lorenz P; Sieland K; Jakob PM; Webb A; Pilgrimm H; Schober R; et al. In Vivo Detection Limits of Magnetically Labeled Embryonic Stem Cells in the Rat Brain Using High-Field (17.6 T) Magnetic Resonance Imaging. NeuroImage 2005, 24, 635–645. [PubMed: 15652299]

(63). Shapiro EM; Sharer K; Skrtic S; Koretsky AP In Vivo Detection of Single Cells by Mri. Magn. Reson. Med 2006, 55, 242–249. [PubMed: 16416426]

(64). Traverse JH; Henry TD; Vaughan DE; Ellis SG; Pepine CJ; Willerson JT; Zhao DX; Simpson LM; Penn MS; Byrne BJ Latetime: A Phase-II, Randomized, Double-Blinded, Placebo-Controlled, Pilot Trial Evaluating the Safety and Effect of Administration of Bone Marrow Mononuclear Cells 2 to 3 Weeks after Acute Myocardial Infarction. Texas Heart Inst. J 2010, 37, 412–420.

(65). Traverse JH; Henry TD; Vaughn DE; Ellis SG; Pepine CJ; Willerson JT; Zhao DX; Piller LB; Penn MS; Byrne BJ; et al. Rationale and Design for Time: A Phase II, Randomized, Double-Blind, Placebo-Controlled Pilot Trial Evaluating the Safety and Effect of Timing of Administration of Bone Marrow Mononuclear Cells after Acute Myocardial Infarction. Am. Heart J 2009, 158, 356–363. [PubMed: 19699857]

(66). Bolli R; Chugh AR; D'Amario D; Loughran JH; Stoddard MF; Ikram S; Beache GM; Wagner SG; Leri A; Hosoda T; et al. Cardiac Stem Cells in Patients with Ischaemic Cardiomyopathy (Scipio): Initial Results of a Randomised Phase 1 Trial. Lancet 2011, 378, 1847–1857. [PubMed: 22088800]

(67). Zhou Z; Lu ZR Gadolinium-Based Contrast Agents for Magnetic Resonance Cancer Imaging. Wiley Interdiscip. Rev.: Nanomed. Nanobiotechnol 2013, 5, 1–18. [PubMed: 23047730]

(68). Tse H-F; Kwong Y-L; Chan JK; Lo G; Ho C-L; Lau C-P Angiogenesis in Ischaemic Myocardium by Intramyocardial Autologous Bone Marrow Mononuclear Cell Implantation. Lancet 2003, 361, 47–49. [PubMed: 12517468]

(69). Aime S; Caravan P Biodistribution of Gadolinium-Based Contrast Agents, Including Gadolinium Deposition. J. Magn. Reson. Imaging 2009, 30, 1259–1267. [PubMed: 19938038]

(70). Niendorf H; Haustein J; Cornelius I; Alhassan A; Clauss W Safety of Gadolinium-Dtpa: Extended Clinical Experience. Magn. Reson. Med 1991, 22, 222–228. [PubMed: 1812350]

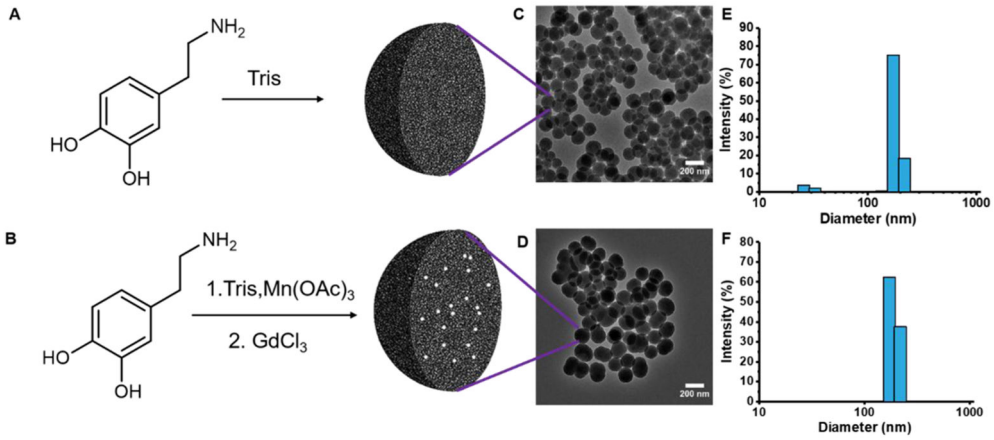

Figure 1.

Synthesis and characterization of synthetic melanin nanoparticles (SMNPs). (A) Molecular structure of dopamine and route to nanoparticles, (B) synthesis of Gd(III)-doped SMNPs, (C) TEM micrograph of SMNPs shows spherical morphology and uniform size, (D) TEM micrograph of Gd(III)-doped SMNPs shows spherical morphology and uniform size, (E) DLS indicates a low dispersity solution and a particle size of 150 nm for SMNPs, (F) DLS data indicate a particle size of 160 nm for Gd(III)-doped SMNPs.

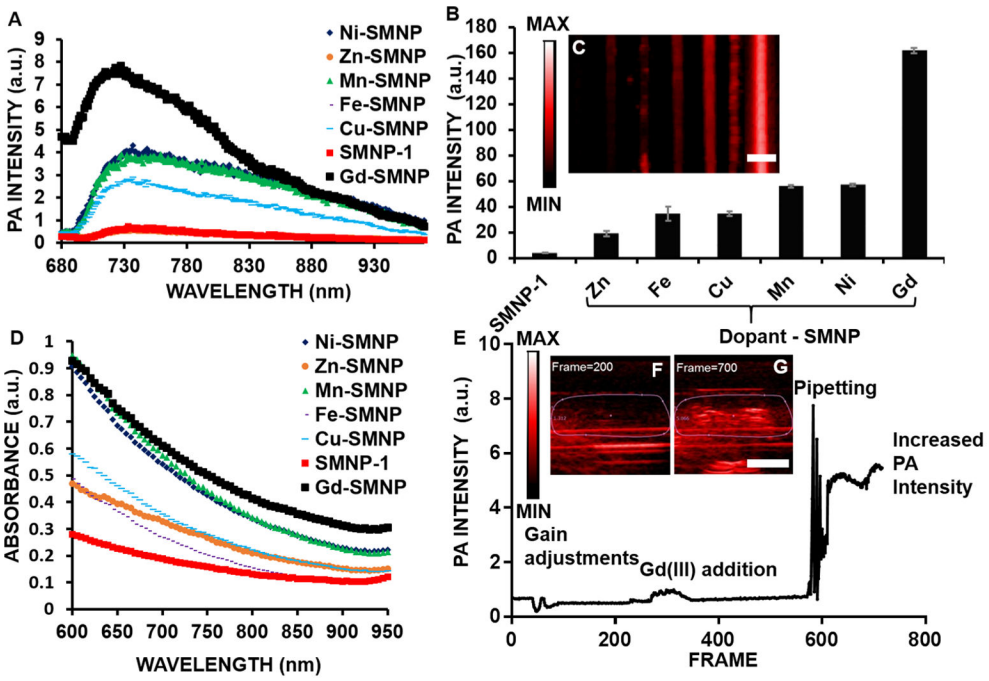

Figure 2.

Photoacoustic (PA) imaging and intensity data of SMNPs and metal-doped SMNPs. (A) Photoacoustic spectra from 680 to 970 nm indicate a broad peak for all nanoparticle samples from 720 to 760 nm. (B) Gd(III)-SMNPs have the highest photoacoustic signal of nanoparticles doped with Ni, Zn, Cu, Mn, Fe, or Gd. The Gd(III)-doped SMNPs showed the highest photoacoustic signal and SMNPs without doping showed the lowest signal. (C) Photoacoustic imaging intensity of SMNPs and metal-doped SMNPs (Ni, Zn, Cu, Mn, Fe, and Gd). (D) Absorbance data of SMNPs and metal-doped (Ni, Zn, Cu, Mn, Fe, Gd-doped) SMNPs indicated that Gd(III) had the highest absorbance from 700 to 950 nm. (E) Quantification of photoacoustic imaging intensity for live exchanging of Mn(III)-SMNPs with Gd(III). Mn(III)-SMNPs were used to increase the Gd(III) loading via Mn–Gd ion exchange to observe the photoacoustic intensity change in real time with mixing via pipetting. The photoacoustic intensity shows a change in signal upon addition of Gd(III) (1 mg/mL) to Mn(III)-doped SMNPs (0.68 mg/mL); (F, G) Snapshots from the in situ photoacoustic movie at frames 200 and 700, respectively. The scale bar in panels C and G represents 4 mm.

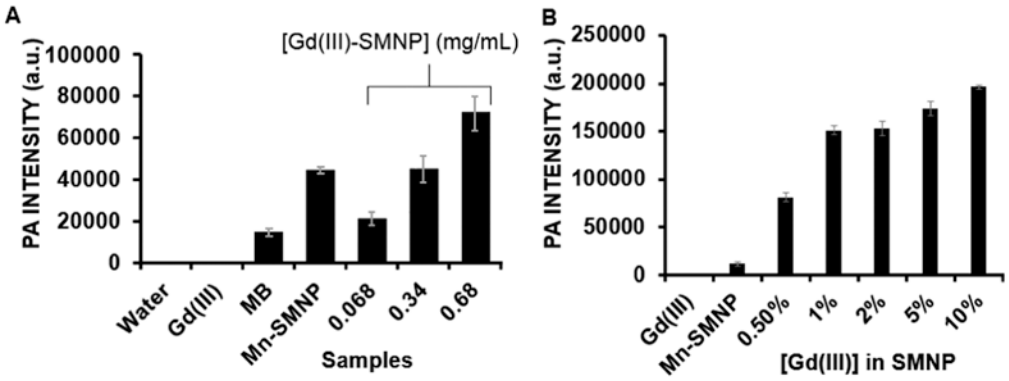

Figure 3.

Photoacoustic (PA) intensity of Gd(III)-doped SMNPs is dependent on the concentration of SMNPs and Gd(III). (A) Photoacoustic intensity data, where 0.68, 0.34, and 0.068 represent the 5% Gd-SMNP concentrations (mg/mL). Mn(III)-SMNPs without Gd(III) doping (0.68 mg/mL), MB (0.4 mM), H_2O, and Gd(III) (40 mg/mL) are controls. (B) Photoacoustic intensity data with constant Mn-SMNP concentration, where 0.5–10% represent the concentration of Gd(III) in Mn-SMNPs. Nanoparticle concentration for all is 0.2 mg/mL. The error bars represent the standard deviation of the ROIs ($n = 8$).

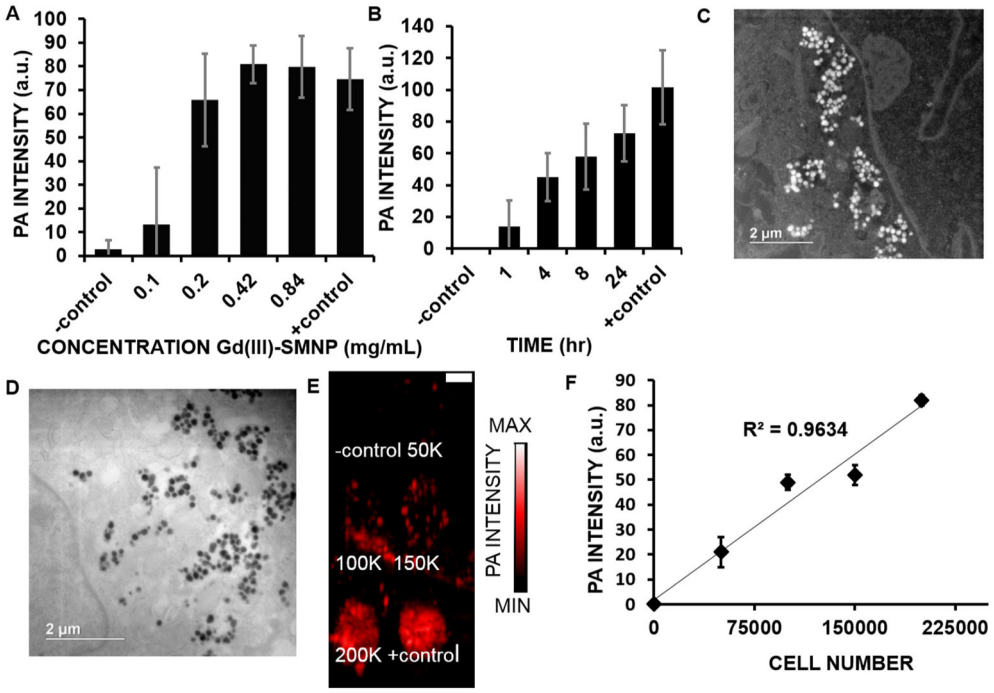

Figure 4.

Optimization of hMSC labeling parameters. (A) Increasing concentrations of nanoparticles (0.1–0.84 mg/mL of Gd(III)-SMNPs) were used to label 150 000 hMSCs; the photoacoustic signal increased accordingly. For panels (A) and (B), unlabeled hMSCs were the negative control. Gd(III)-SMNPs (0.152 μmol/mL Gd(III)) were the positive control. (B) The effect of incubation time on photoacoustic intensity of 150 000 hMSCs treated with 0.42 mg/mL of Gd(III)-SMNPs. The photoacoustic intensity increased as time increased from 1 to 24 h. *Indicates p-value <0.05. (C) Dark-field scanning transmission electron microscopy (STEM) of hMSCs treated with Gd(III)-SMNPs (4 h, 0.42 mg/mL), where the white dots indicate the Gd(III)-SMNPs. (D) TEM microscopy of hMSCs treated with Gd(III)-SMNPs (4 h, 0.42 mg/mL), where the black dots indicate the Gd(III)-SMNPs. (E) Photoacoustic imaging data of hMSCs labeled with Gd(III)-SMNPs. The photoacoustic intensity increased upon increasing the incubation time from 1 to 24 h, suggesting increased internalization of the particles with increasing time. The scale bar represents 1 cm. (F) Photoacoustic intensity data of 0–200 000 hMSCs labeled with Gd(III)-SMNPs showed a linear relationship between cell number and photoacoustic intensity.

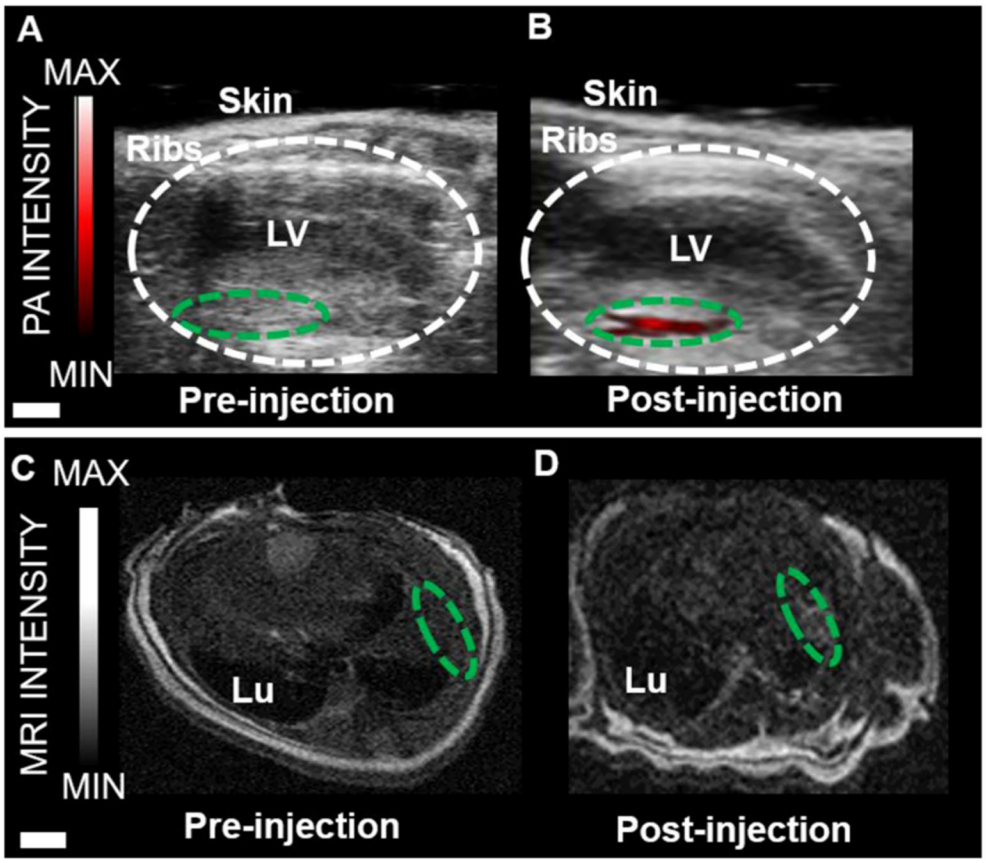

Figure 5.

Photoacoustic and MR imaging of Gd(III)-SMNPs-labeled hMSCs implanted into mouse hearts. (A) Photoacoustic imaging of the longitudinal axis view of live mouse heart pre-injection. The area circled in white represents the left ventricle (LV). The area circled in green represents the area of the left ventricle wall before injection. (B) Photoacoustic imaging of the longitudinal axis view of a live mouse heart post-injection. For this, 500 000 hMSCs labeled with Gd(III)-SMNPs were injected. The green-circled area shows the increase in photoacoustic imaging intensity (red). (C) Transverse MRI view of a mouse heart pre-injection. The green-circled area represents the LV wall. Lu is the lung. (D) Transverse MRI view of a mouse heart post-injection. For this, 500 000 hMSCs labeled with Gd(III)-SMNPs were injected. The green-circled area shows the increase in MRI signal intensity in the LV wall. The scale bar in A and B represents 2 mm; the scale bar for C and D represents 5 mm.

Table 1.

ICP-OES Measurements of Metal-Doped SMNPs[a]

sample	metal loading (wt %)
Mn(III)-doped SMNPs	6.0
Fe(III)-doped SMNPs	5.9
Ni(II)-doped SMNPs	5.9
Cu(II)-doped SMNPs	6.2
Zn(II)-doped SMNPs	8.3
Gd(III)-doped SMNPs	6.4

[a]Metal loading varies from 5.9 to 8.3% by weight for metal-doped SMNP samples.